nuclear fusion
IAEA

PAPER • OPEN ACCESS

Halo current rotation scaling in post-disruption plasmas

To cite this article: A.R. Saperstein *et al* 2022 *Nucl. Fusion* **62** 026044

View the article online for updates and enhancements.

You may also like

- Inter-code comparison benchmark between DINA and TSC for ITER disruption modelling
S. Miyamoto, A. Isayama, I. Bandyopadhyay et al.
- Characterization of disruption halo currents in the National Spherical Torus Experiment
S.P. Gerhardt, J. Menard, S. Sabbagh et al.
- Characterization of disruption halo current between 'W-Like' graphite divertor and 'ITER-Like' divertor structure on EAST tokamak
D L Chen, R S Granetz, L Zeng et al.

This content was downloaded from IP address 1.27.104.22 on 03/11/2023 at 09:27

OPEN ACCESS
IOP Publishing | International Atomic Energy Agency Nuclear Fusion
Nucl. Fusion **62** (2022) 026044 (6pp) https://doi.org/10.1088/1741-4326/ac4186

Halo current rotation scaling in post-disruption plasmas

A.R. Saperstein*, J.P. Levesque, M.E. Mauel and G.A. Navratil

Department of Applied Physics and Applied Mathematics, Columbia University, New York, NY 10027, United States of America

E-mail: alex.saperstein@columbia.edu

Received 21 September 2021, revised 17 November 2021
Accepted for publication 9 December 2021
Published 6 January 2022

Abstract

Halo current (HC) rotation during disruptions can be potentially dangerous if resonant with the structures surrounding a tokamak plasma. We propose a drift-frequency-based scaling law for the rotation frequency of the asymmetric component of the HC as a function of toroidal field strength and plasma minor radius ($f_{\rm rot} \propto 1/B_{\rm T}a^2$). This scaling law is consistent with results reported for many tokamaks and is motivated by the faster HC rotation observed in the HBT-EP tokamak. Projection of the rotation frequency to ITER and SPARC parameters suggest the asymmetric HC rotation will be on the order of 10 Hz and 60 Hz, respectively.

Keywords: tokamak, HBT-EP, scaling law, disruption, halo current, rotation

(Some figures may appear in colour only in the online journal)

1. Introduction

Damage to the vacuum vessel (VV) and other integral components due to electromagnetic (EM) loads during disruption events is a concern for high current tokamak devices, which are susceptible to strong currents, called halo currents (HCs), that can be exchanged between the VV and the plasma edge during disruptions [1–3]. These HCs can have significant toroidal asymmetries [4–12] in addition to their axisymmetric components, and when their poloidal component is crossed with the toroidal field, it can lead to large asymmetric sideways forces on the VV and other mechanical components [4, 13]. These asymmetric HCs have been observed to rotate when $q_{\rm edge}$ falls below 2 [4, 9], with rotation frequencies ranging from 100 s of Hz to 10 s of kHz among machines of various sizes [20]. These HC rotations can be especially concerning if their rotation frequency nears that of any of the vessel's natural resonant frequencies, significantly amplifying the damaging effects of the EM loads if two or more revolutions are made.

Progress has been made in understanding and simulating axisymmetric HCs [14, 15]; however, much less is understood about the rotation dynamics of their asymmetric components [16–18]. Attempts to understand the physics of the rotation through theoretical means have been proposed [19], but have not been experimentally verified. To date, only an empirical prediction for the rotation frequency of asymmetric HCs has been proposed using observations from multiple mid-to-large-scale tokamaks [20]. While the existing projections are also accurate enough to describe some disruption characteristics on the smaller-scale HBT-EP tokamak [12], like its current quench (CQ) duration, they can under-predict the frequencies of the fast rotating HCs observed by more than an order of magnitude. Additionally, the existing empirical scaling only considers average rotation frequencies, and does not consider the evolution of the rotation frequency throughout the CQ, which has been seen to be significant on HBT-EP and other devices [20].

Here, we propose an alternative scaling law for the post-disruption rotation frequency ($f_{\rm rot}$) based on a drift frequency scaling ($\propto 1/B_{\rm T}a$) and the assumption of a common inter-machine post-thermal quench temperature, that leads to another factor that depends primarily on the inverse minor radius and only weakly on other parameters. This alternate scaling law describes the rotation frequency as

* Author to whom any correspondence should be addressed.

Original content from this work may be used under the terms of the Creative Commons Attribution 4.0 licence. Any further distribution of this work must maintain attribution to the author(s) and the title of the work, journal citation and DOI.

 © 2022 The Author(s). Published on behalf of IAEA by IOP Publishing Ltd

$$f_{\text{rot}} \sim \frac{A}{B_{\text{T}} a^2}, \tag{1}$$

where B_{T} is the strength of the toroidal field, a is the minor radius, and A is a constant that varies weakly with other machine parameters. Equation (1) suggests the HC rotation is proportional to the $E \times B$ and electron diamagnetic poloidal rotations in the post-disruption plasma. The validity of this empirical scaling law is verified through comparisons between several tokamaks with rotation frequencies that vary over three orders of magnitude, as well as its ability to describe the evolution of the rotation frequency over the course of individual disruptions on HBT-EP, as the minor radius, a, decreases.

The remainder of this paper is organized into three additional sections. Section 2 illustrates the good agreement of this scaling law between multiple machines, and establishes its validity over several orders of magnitude in scale-factor and frequency. Section 3 then discusses and summarizes observations of the HC rotation during the post-disruption CQ on HBT-EP. These observations demonstrate that the scaling in equation (1) can be used to accurately describe the evolution of the rotation frequency over the course of the CQ on HBT-EP. Finally, section 4 discusses the application of this scaling law in further detail.

2. Multi-machine scaling

A multi-machine comparison of post-disruption rotation frequencies and their corresponding scale-factors for disruptions on JET [4, 5], C-Mod [6], DIII-D [7], AUG [8], NSTX [9], KSTAR [10], COMPASS [5, 11], and HBT-EP [12] can be found in figure 1. Toroidal fields and minor radii are approximated using typical pre-disruption plasma parameters for the given device, and an approximate disruption rotation frequency is estimated based on reported HC rotation frequencies. Table 1 provides a more detailed description of the sources for the data-points used in figure 1.

A linear fit of the data shows that there is a clear correlation between rotation frequency and the proposed scale-factor over three orders of magnitude and eight devices of widely varying toroidal fields and sizes. The scaling constant (A), is estimated to be about 237 (Hz T m^2). Even the fast post-disruption rotation frequencies seen on HBT-EP, which do not fit the scaling law proposed by Myers *et al* [20], are in good agreement with this proposed scaling. This is especially significant given that the characteristic scale-factors and rotation frequencies for HBT-EP are an order of magnitude larger than that of the next machine, which lends credibility to this scaling law's ability to predict the rotation frequencies over several orders of magnitude.

A prediction to larger tokamaks with smaller scale factors, like ITER, shows that the HC rotation frequency will be significantly slower than in existing devices. With ITER's design parameters [21], the scaling indicates HC rotation near 10 Hz, which is potentially dangerous for EM loads [2]. The scaling law proposed by Myers and co-authors [20] suggest that ITER's rotation frequencies could be as small as 10 s of Hz, but also that they could be as high as 100 s of Hz. While both scaling laws suggest potential dangerous rates of HC rotation, this new proposed scaling leverages a wider range of disruption parameters and may lead to improved understanding of HC rotation processes.

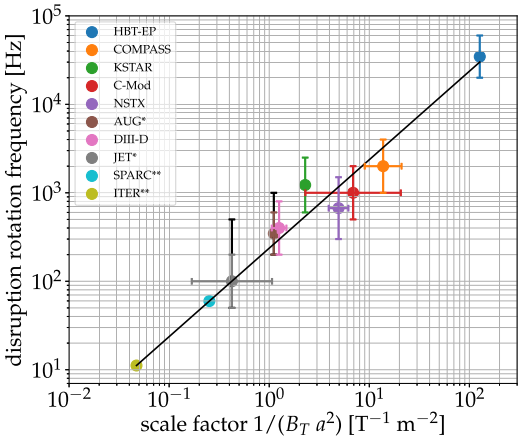

Figure 1. Typical disruption rotation frequencies across multiple machines, characterized by their corresponding approximate scale-factors, given by the denominator in equation (1). See table 1 for a description of each data-point. The black curve is a linear fit of the average frequencies for each machine. *The colored spreads in JET and AUG data represent their carbon wall data-sets, while the black spreads (in addition to their colored spreads) includes their metal wall data-sets. Only the carbon wall datasets were included in the fit for these devices. **A typical rotation frequency for SPARC is projected (∼60 Hz) using the linear fit, with nominal SPARC parameters [22] used to estimate its scale-factor; a similar rotation frequency is projected for ITER (∼10 Hz), with nominal ITER parameters provided by [21].

3. Rotation frequency evolution on HBT-EP

While section 2 demonstrates the validity of this scaling law between various machines over several orders of magnitude in frequency, only pre-disruption parameters were used to define a scale-factor that characterizes a post-disruption frequency. Measurements of the HC rotation frequency and minor radius during individual disruptions on HBT-EP improve the validity of this scaling law by establishing a post-disruption scale-factor that characterizes a dynamic post-disruption rotation frequency. Disruptions are often characterized by a decrease in minor radius, and this scaling law reflects this in HBT-EP through an increase in HC rotation frequency throughout the evolution of the CQ. HBT-EP is particularly useful for this study, since it lacks many of the features common on larger devices which may require higher-order corrections. Namely, it lacks potential torques/drags driven by external effects like NBI and pellet/gas injection, and it has a relatively simple circular limited plasma cross-section, which helps to avoid any ambiguity in defining a minor radius for the scale-factor.

Figure 2 shows the evolution of the plasma over the course of a typical disruption on HBT-EP. A detailed description of the HBT-EP experiment and the diagnostics available can be found in reference [12]. For the purposes of this study, the diagnostics of interest are the HC sensors, which measure current in the vessel moving toroidally through jumper cables between

Table 1. Reported post-disruption HC rotation frequencies and pre-disruption machine parameters used in the multi-machine scaling shown in figure 1. An average rotation frequency ($\langle f_{\rm rot}\rangle$) and toroidal field ($\langle B_{\rm T}\rangle$) was chosen for each machine based on the average in log-space of the corresponding reported spreads. The characteristic scale-factor for each device is estimated using these average parameters.

Machines	$\langle f_{\rm rot}\rangle$ (Hz)	$f_{\rm rot}$ spread (Hz)	$\langle B_{\rm T}\rangle$ (T)	$B_{\rm T}$ spread (T)	a (m)	Scale-factor ($\rm T^{-1}\ m^{-2}$)
HBT-EP[a]	34 600	$20\,000 \rightarrow 60\,000$	0.35	—	0.15	127.0
COMPASS[b]	2000	$1000 \rightarrow 4000$	1.5	$0.9 \rightarrow 2.1$	0.23	13.8
KSTAR[c]	1220	$600 \rightarrow 2,500$	1.75	$1.7 \rightarrow 1.8$	0.5	2.3
C-Mod[d]	1000	$500 \rightarrow 2000$	5	$1 \rightarrow 9$	0.22	6.9
NSTX[d]	670	$300 \rightarrow 1500$	0.55	$0.35 \rightarrow 0.55$	0.68	4.9
AUG[d,e]	447	$200 \rightarrow 1000$	2.5	—	0.6	1.1
DIII-D[d]	400	$200 \rightarrow 800$	2.0	$1.5 \rightarrow 2.1$	0.67	1.3
JET[d,e]	100	$50 \rightarrow 500$	3	$0.6 \rightarrow 3.8$	1.25	0.4
SPARC[f]	60	—	12.2	—	0.57	0.25
ITER[g]	10	—	5.3	—	2	0.05

[a]Average rotation frequency and spread seen on HBT-EP. There is no significant spread in the toroidal field for HBT-EP.
[b]Average rotation frequency and toroidal field, along with corresponding spread in data reported by references [5, 11].
[c]Average rotation frequency and toroidal field, along with corresponding spread in data reported by reference [10].
[d]Average rotation frequency and spread in data reported by reference [20]. Toroidal field spread information reported by reference [4] (JET), [6] (C-Mod), [7] (DIII-D), and [9] (NSTX).
[e]The JET and AUG data shown here consider observations during both carbon wall (JET-C/AUG-C) and metal wall operation (JET-ILW/AUG-W).
[f]Design parameters for SPARC provided by [22]. Projected $\langle f_{\rm rot}\rangle$ based on fit to scaling law seen in figure 1.
[g]Design parameters for ITER provided by [21]. Projected $\langle f_{\rm rot}\rangle$ based on fit to scaling law seen in figure 1.

vessel sections that are otherwise insulated from each other, meaning they are a direct measure of the total toroidal current flowing in the vessel at their respective toroidal positions. The fluctuations in the signal of one of these sensors is used to establish the HC rotation frequency (figure 2(f)), which is found to correlate well with the frequencies in other HC sensors, as well as the in-vessel magnetic sensors (figure 2(e)).

Disruptions occur with nearly every discharge on HBT-EP and typically have the following characteristics shown in figure 2. A disruption is triggered with the onset of one or more large rotating $n = 1$ MHD mode(s) and a sudden increase in visible radiation. A current-spike occurs ($\sim$7 ms in figure 2) and the plasma major radius moves inboard. As the CQ continues, the major radius moves further inward below 0.9 m, causing the minor radius to decrease as the plasma limits on the high-field side. During the CQ, HCs reach about 5% of the plasma current and have both a time-averaged and fluctuating component which are comparable to each other. The time-averaged component of the current is always observed to be in the co-$I_{\rm p}$ direction. Based on correlations with magnetic fluctuations, the fluctuating component always rotates in the electron diamagnetic direction.

The most notable characteristic of HBT-EP disruptions is that the rotation frequency (of both the HCs and the magnetics) increases quickly over the duration of the CQ (figure 2(g)). This shows how the change in frequency correlates with the change in the instantaneously measured scale-factor. Figure 3 shows a 2D-histogram of instantaneous rotation frequencies vs scale-factors for the disruptions of 64 shots, sampled every 2 μs (diagnostic sampling frequency). The analyses were performed over the periods of the disruptions corresponding to the fall of plasma current from 80% to 20% of its pre-disruption value (to be consistent with the existing convention used in reference [20]), with the exception that data-points were only included when the major radius was above some threshold value while the measurement of the major radius was valid. This threshold major radius value corresponds to a minor radius about 0.08 m (about 57% the maximum pre-disruption minor radius), and this allowed for measurement of the dynamic scale-factor to range from $1 \rightarrow 3$ times its minimum pre-disruption value.

In figure 3, we see a linear growth in frequency as the scale-factor increases (and the minor radius decreases). A linear least-squares fit was performed on the data, and the empirical constant, A, for the scaling law was estimated to be about 110 (Hz T $\rm m^2$). This constant is different only by a factor of $\sim$2 from the constant estimated for the multi-machine scaling law, which was based on the pre-disruption parameters and was found to be about 237 (Hz T $\rm m^2$). The frequency predicted by this scaling law using the HBT-EP-specific A constant and the measured scale-factor can be seen plotted against the measured rotation frequency in figure 2(g) (blue), which shows good agreement over the course of the CQ, even prior to the $80\% \rightarrow 20\%$ window.

4. Discussion

We propose a new scaling law for characterizing post-disruption HC rotation frequencies in proportion to $1/B_{\rm T}a^2$. This proposed scaling law is empirically validated with observations reported by several tokamaks. When including HC rotation measurements from HBT-EP, the scaling law is shown to be comparable to observations over several orders of magnitude. This proposed scaling law extends the range of validity as compared to the scaling proposed in reference [20]. Additionally, because HC rotation scales with the drift parameter, $1/B_{\rm T}a^2$, this scaling motivates a physical reason for HC rotation. Finally, we show that for disruptions like those in

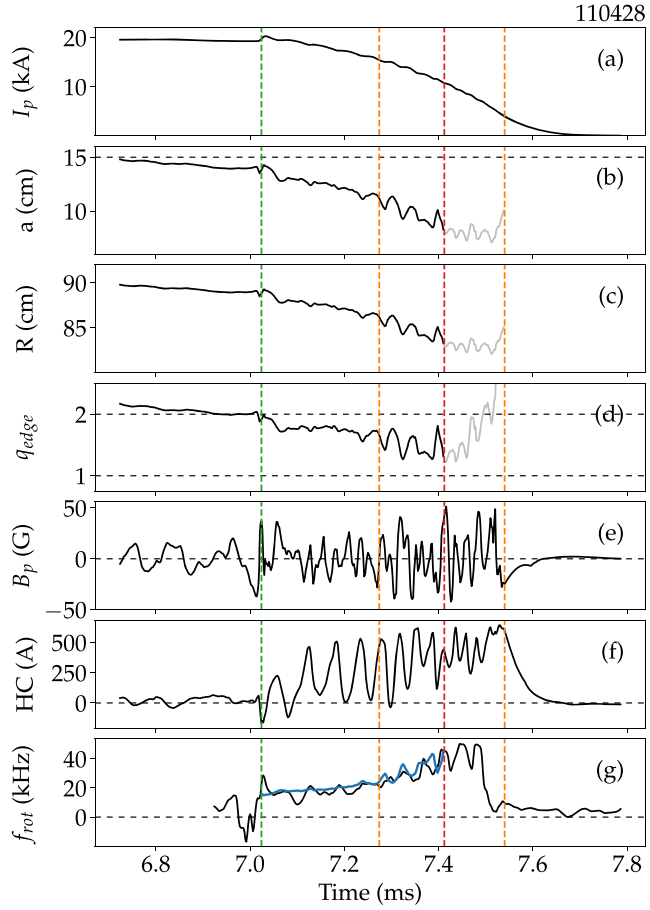

Figure 2. Plasma signals during a typical disruption evolution on HBT-EP: (*a*) plasma current, (*b*) minor radius, (*c*) major radius (current centroid), (*d*) edge safety factor, (*e*) a poloidal magnetic field sensor (filtered above 5 kHz), (*f*) toroidal vessel HC at one toroidal location, (*g*) rotation frequency of the toroidal HC (black) and the rotation frequency estimated using the proposed scaling law (blue). The green dashed line is the time of the current spike, defined as the 'disruption event'. The orange dashed lines represent the t_{80} and t_{20} times, where I_p has fallen to 80% and 20% of its pre-disruptive values. The red dashed line is the time where the analysis is cutoff, due to the major radius dropping too low to reliably measure the minor radius.

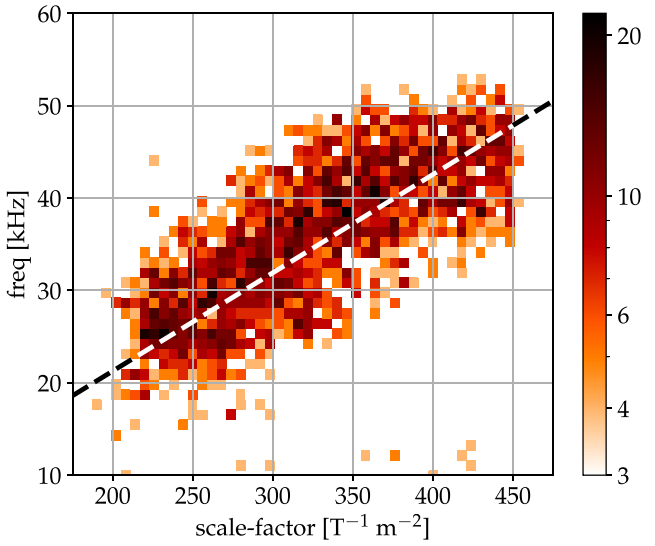

Figure 3. 2D-histogram of HC rotation frequency vs scale-factor for more than 6000 data-points taken over 64 disruptions on HBT-EP. The color-scale is logarithmically normalized. The dashed line is linear fit to the data.

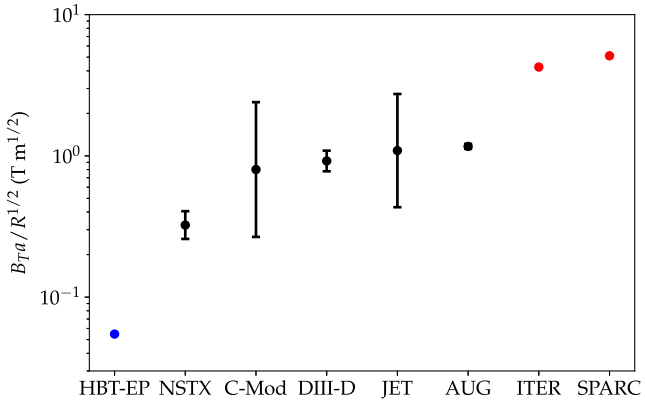

Figure 4. Difference factor between Myers *et al*'s scale-factor and the proposed proposed scale-factor, plotted for the machines considered in Myers *et al*'s database (black), as well as HBT-EP (blue), and ITER and SPARC (red).

HBT-EP, this new scaling law is capable of describing dynamic changes in the rotation frequency.

The most notable difference between this proposed scaling law and previous attempts is the significance of the toroidal field, B_T. Myers *et al* [20] emphasize that their scaling was insensitive to the addition of the toroidal field as a fitting parameter, but this may be because the variance in B_T among the machines in their database are approximately compensated for by comparable changes in other variables, namely $R^{1/2}/a$, that together characterize the difference between the Myers scaling and the proposed scaling, $f_{\rm rot}^{\rm Myers}/f_{\rm rot} \approx B_T a/R^{1/2}$. The approximate invariance of $B_T a/R^{1/2}$ in the Myers *et al* database is shown as black data points in figure 4. This may lead to the toroidal field being absorbed into Myers' scaling pre-factor, $A_{\rm Myers}$ (called C_f in reference [20]). The addition of HBT-EP to the Myers *et al* database adds significant variance to the $B_T a/R^{1/2}$ factor, and therefore highlights the role of the toroidal field. This is seen in the fact that the Myers *et al* scaling law under-predicts the rotation frequencies on HBT-EP by an order of magnitude, while the proposed scaling does not, as shown in figure 5.

The wall material also affects the spread in rotation frequencies. Both JET and AUG observe larger spreads in frequencies during their metal wall operations than in their carbon wall counterparts, and are slightly faster on average [20]. This increase in rotation frequency is also accompanied by an observed increase in post-thermal quench (TQ) temperatures [23, 24], which may contradict the common post-TQ T_e assumption and explain the deviation from the proposed scaling. An increase in rotation frequency with post-TQ T_e is also consistent with the drift force being proportional to the radial electron temperature gradient ($\partial T_e/\partial r$), which is one possible physical interpretation of the scaling law. If so, the temperature-independent version of the scaling law would

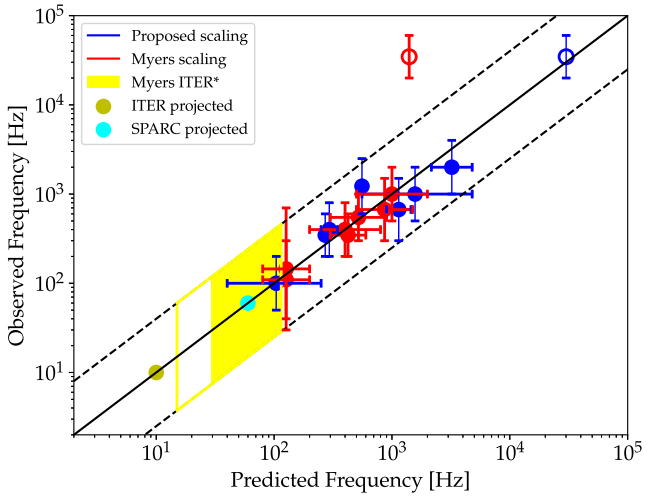

Figure 5. Observed HC rotation frequencies plotted against scaling law predictions for the Myers *et al* scaling (red) and the proposed scaling law (blue). The HBT-EP data-points are open circles, while all others are closed. The yellow window is the range of frequencies projected in Myers *et al* [20] for ITER, and the dashed black lines represent the error bounds they used. The predicted SPARC and ITER rotation frequencies, using the proposed scaling, are also plotted (cyan and dark yellow respectively).

remain adequate for comparing machines with similar wall materials, or more specifically, similar post-TQ temperatures. A temperature-dependent version of the scaling that bridges the physics of dissimilar-wall machines could also be introduced, and motivates the development of a thorough post-TQ T_e database. The increase in rotation frequency from carbon to metal wall machines suggests that ITER's rotation frequency will be larger than that predicted by the carbon-wall fit, but JET and AUG carbon-to-metal wall comparisons suggest the difference will only be on the order of a factor of 2.

The time evolution of the HC rotation frequency on HBT-EP demonstrates that this scaling law is less sensitive to variations in predicted frequencies and captures the primary underlying physics driving rotation during the CQ. While restricting the analysis to providing only a single rotation frequency to each disruption for the purpose of empirical fitting is useful for demonstrating the validity of the scaling law over large scales (like that done in reference [20] and figure 1), shot-to-shot variations in disruption dynamics inevitably lead to uncertainties in the predictions of the scaling law. By comparison, as shown in figure 3, this new scaling law, when applied dynamically, can accurately describe the rotation frequency with up to five-fold less uncertainty and to within a factor of about two on HBT-EP. Furthermore, the increasing frequency of the post-disruption HC rotation as the minor radius decreases gives evidence supporting the mechanism for HC rotation involves poloidal, not toroidal, rotation.

There is also good agreement between the scaling pre-factor constants calibrated using the multi-machine scaling and the HBT-EP disruption evolution scaling, to within a factor of 2–3. This suggests that physics governing the evolution of the rotation frequency over the course of the CQ is similar to the physics describing the variance in rotation frequency between machines.

Acknowledgement

This work was supported by U.S. Department of Energy, Office of Science, Office of Fusion Energy Science, Grant DE-FG02-86ER53222.

ORCID iDs

A.R. Saperstein https://orcid.org/0000-0001-7111-1961
J.P. Levesque https://orcid.org/0000-0003-1193-475X
M.E. Mauel https://orcid.org/0000-0003-2490-7478
G.A. Navratil https://orcid.org/0000-0002-2930-5196

References

[1] Hender T.C. *et al* 2007 Progress in the ITER Physics Basis Chapter 3: MHD stability, operational limits and disruptions *Nucl. Fusion* **47** S128–S202
[2] Schioler T., Bachmann C., Mazzone G. and Sannazzaro G. 2011 Dynamic response of the ITER tokamak during asymmetric VDEs *Fusion Eng. Des.* **86** 1963–6
[3] Albanese R. *et al* 2015 Effects of asymmetric vertical disruptions on ITER components *Fusion Eng. Des.* **94** 7–21
[4] Gerasimov S.N., Hender T.C., Morris J., Riccardo V. and Zakharov L.E. 2014 *Nucl. Fusion* **54** 073009
[5] Gerasimov S.N. *et al* 2015 *Nucl. Fusion* **55** 113006
[6] Granetz R.S., Hutchinson I.H., Sorci J., Irby J.H., LaBombard B. and Gwinn D. 1996 *Nucl. Fusion* **36** 545
[7] Evans T.E., Kellman A.G., Humphreys D.A., Schaffer M.J., Taylor P.L., Whyte D.G., Jernigan T.C., Hyatt A.W. and Lee R.L. 1997 *J. Nucl. Mater.* **241–243** 606–11
[8] Pautasso G., Giannone L., Gruber O., Herrmann A., Maraschek M. and Schuhbeck K.H. 2011 *Nucl. Fusion* **51** 043010
[9] Gerhardt S.P. 2013 *Nucl. Fusion* **53** 023005
[10] Bak J.G. 2016 Characteristics of halo current in the KSTAR tokamak *Proc. 26th IAEA Fusion Energy Conf.* (Kyoto, Japan) (https://nucleus.iaea.org/sites/fusionportal/Shared%20Documents/FEC%202016/fec2016-preprints/preprint0689.pdf)
[11] Matveeva E. *et al* 2018 Statistical analysis of disruptions in COMPASS *WDS'18 Proc. Contributed Papers—Physics* pp 105–11 (https://www.mff.cuni.cz/veda/konference/wds/proc/proc-contents.php?year=2018)
[12] Levesque J.P. *et al* 2017 *Nucl. Fusion* **57** 086035
[13] Roccella R., Roccella M., Riccardo V. and Chiocchio S. 2016 Asymmetric toroidal eddy currents (ATEC) to explain sideways forces at JET *Nucl. Fusion* **56** 106010
[14] Artola F.J., Sovinec C.R., Jardin S.C., Hoelzl M., Krebs I. and Clauser C. 2021 3D simulations of vertical displacement events in tokamaks: a benchmark of M3D-C1, NIMROD, and JOREK *Phys. Plasmas* **28** 052511
[15] Yanovskiy V.V. *et al* 2021 Global forces on the COMPASS-U wall during plasma disruptions *Nucl. Fusion* **61** 096016
[16] Strauss H., Sugiyama L., Paccagnella R., Breslau J. and Jardin S. 2014 Tokamak toroidal rotation caused by AVDEs and ELMs *Nucl. Fusion* **54** 043017

[17] Manickam J., Boozer A. and Gerhardt S. 2012 Kink modes and surface currents associated with vertical displacement events *Phys. Plasmas* **19** 082103
[18] Zakharov L.E., Galkin S.A. and Gerasimov S.N. (JET-EFDA Contributors) 2012 Understanding disruptions in tokamaks *Phys. Plasmas* **19** 055703
[19] Boozer A.H. 2012 *Phys. Plasmas* **19** 052508
[20] Myers C.E., Eidietis N.W., Gerasimov S.N., Gerhardt S.P., Granetz R.S., Hender T.C. and Pautasso G. 2018 *Nucl. Fusion* **58** 016050
[21] Aymar R., Barabaschi P. and Shimomura Y. 2002 *Plasma Phys. Control. Fusion* **44** 519
[22] Creely A.J. *et al* 2020 *J. Plasma Phys.* **86** 865860502
[23] Matthews G.F. 2013 *J. Nucl. Mater.* **438** S2–S10
[24] Neu R.L. *et al* 2014 *IEEE Trans. Plasma Sci.* **42** 552–62